Takahiro Iwamoto,*[a] Sota Amano,[a] Kousuke Maeda,[b] Natsuki Shibama,[b] Wakana Sekiguchi,[b] Yuki Kazama,[b] Yasuyuki Nakamura,[c] Koh Sugamata,[d] Hiroaki Imoto,[a] Kensuke Naka,[a] and Youichi Ishii[b]

E-mail: tiwamoto@kit.ac.jp

Contents

1. General Considerations

All manipulations were carried out under an argon or a nitrogen atmosphere. ^{1}H NMR spectra were recorded on a Varian Mercury 400 spectrometer (400 MHz) or a JEOL ECA-500 spectrometer (500 MHz). ^{13}C{^{1}H} (125 or 100 MHz) spectra were recorded on a JEOL ECA-500 spectrometer. The ^{1}H chemical shifts are reported in ppm (δ) from internal tetramethylsilane. The ^{13}C chemical shifts are referenced to signals of $CDCl_3$ (δ 77.16). Gel permeation chromatography (GPC) was performed on JAIGEL 1H and 2H polystyrene columns (Japan Analytical Industry Co., Ltd.) with $CHCl_3$ as the eluent. High-resolution mass spectra were measured by matrix-assisted laser-desorption ionization (MALDI) TOF MS on a spectrometer in the positive reflection mode and at 20 kV acceleration voltage. Solid-state IR spectra were recorded using a Nicolet 6700 FT-IR spectrometer equipped with a Smart-Orbit (Diamond) attenuated total reflection (ATR) accessory.

2. Synthetic Experimental

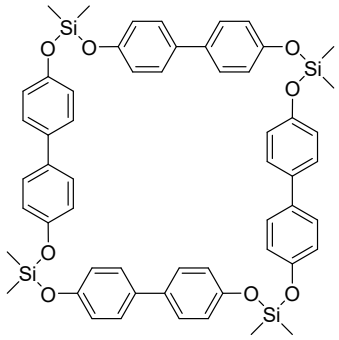

Synthesis of macrocycle 2

To a solution of 4,4'-dihydroxybiphenyl (93.5 mg, 0.502 mmol) and imidazole (68.7 mg, 1.01 mmol) in THF (1.0 mL) was added dichlorodimethylsilane (60 μL, 0.50 mmol). After the mixture was stirred at room temperature for 10 mins, the resulting suspension was filtered, and the solid was washed with THF. The solvent was removed under reduced pressure to afford the almost pure title product as a colorless solid (121.6 mg, 0.125 mmol) in 99% yield. Note that water contamination greatly reduces the macrocyclization efficiency. The product can be further purified by GPC, if necessary, although the ^{1}H NMR signals after purification by GPC were consistent with those of the crude compound. A single crystal for X-ray analysis was obtained by slow evaporation of Et_2O solution of the product.
^{1}H NMR ($CDCl_3$) δ 7.43 (d, J = 8.8 Hz, 16H), 7.01 (d, J = 8.8 Hz, 16H), 0.41 (s, 24 H); ^{13}C NMR ($CDCl_3$) δ 153.5, 134.8, 128.1, 120.2, −2.15; ^{29}Si NMR ($CDCl_3$) δ −5.20; MS (MALDI-TOF): *m/z* $[M]^+$ calcd for $C_{56}H_{56}O_8Si_4$ 968.30522, found 968.30538; IR (ATR): ν = 1602, 1490, 1232, 1166, 914, 821, 800, 711 cm^{-1}. mp: 149-162 °C.

Syntheses at High Concentration (3.0 M)

To a solution of 4,4'-biphenol (112. mg, 0.604 mmol) and imidazole (82.1 mg, 1.21 mmol) in THF (0.20 mL) was added dichlorodimethylsilane (72 μL, 0.60 mmol) at −38 °C. The mixture was stirred at room temperature for 1h. The resulting white suspension was filtered through a short pad of Celite, and the pad was washed with THF (ca. 3 ml). The solvent was removed under reduced pressure to afford compound **2** in 97% yield.

Synthesis of macrocycle 4

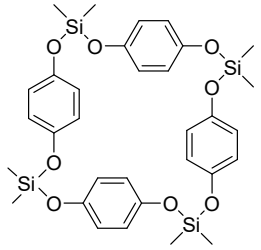

To a solution of hydroquinone (55.2 mg, 0.501 mmol) and imidazole (68.6 mg, 1.00 mmol) in THF (1.0 mL) was added dichlorodimethylsilane (60 μL, 0.50 mmol). After the mixture was stirred at room temperature for 1 h, the resulting suspension was filtered, and the solid was washed with THF. The solvent was removed under reduced pressure to afford the title product as a colorless solid (80.7 mg, 0.121 mmol) in 97% yield. A single crystal for X-ray analysis was obtained by slow evaporation of Et_2O solution of the product.

^{1}H NMR ($CDCl_3$) δ 6.79 (s, 16H), 0.31 (s, 24H); ^{13}C NMR ($CDCl_3$) δ 149.0, 120.6, −2.23; ^{29}Si NMR ($CDCl_3$) δ −5.55; MS (MALDI-TOF): *m/z* $[M+H]^+$ calcd for $C_{32}H_{41}O_8Si_4$ 665.1873, found 665.1864; IR (ATR): ν = 1494, 1209, 912, 798, 521, 403 cm^{-1}. mp: 95-118 °C.

Synthesis of macrocycle 6

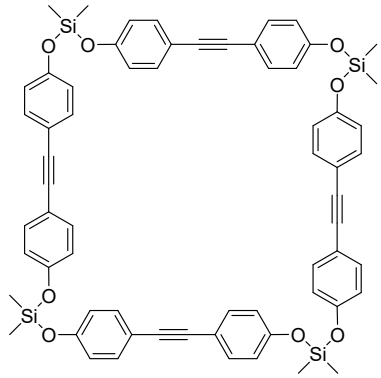

To a solution of diol **5** (63.1 mg, 0.300 mmol) and imidazole (40.8 mg, 0.599 mmol) in THF (0.6 mL) was added dichlorodimethylsilane (36 μL, 0.301 mmol). After the mixture was stirred at room temperature for 0.5 h, the resulting suspension was filtered, and the solid was washed with THF. The solvent was removed under reduced pressure. The filtrate was suspended with CH_3CN, and the suspension was kept for 10 mins. After filtration, the solid was washed with CH_3CN to afford the title product as a colorless solid in 97% yield (77.6 mg, 0.073 mmol).

^{1}H NMR ($CDCl_3$) δ 7.41 (d, J = 8.4 Hz, 16H), 6.91 (d, J = 8.4 Hz, 16H), 0.40 (s, 24H); ^{13}C NMR ($CDCl_3$) δ 154.1, 133.2, 120.1, 117.4, 88.4, −2.11; ^{29}Si DEPT NMR ($CDCl_3$) δ −4.31; MS (MALDI-TOF): *m/z* $[M]^+$ calcd for $C_{64}H_{56}O_8Si_4$ 1064.30468, found 1064.30469; IR (ATR): ν = 3040, 2963, 1603, 1508, 1409, 1312, 1235, 1164, 1099, 909, 833, 799, 728, 700 cm^{-1}. A melting point was not observed in the TGA analysis, likely due to the formation of an amorphous state.

Optimization of reaction conditions

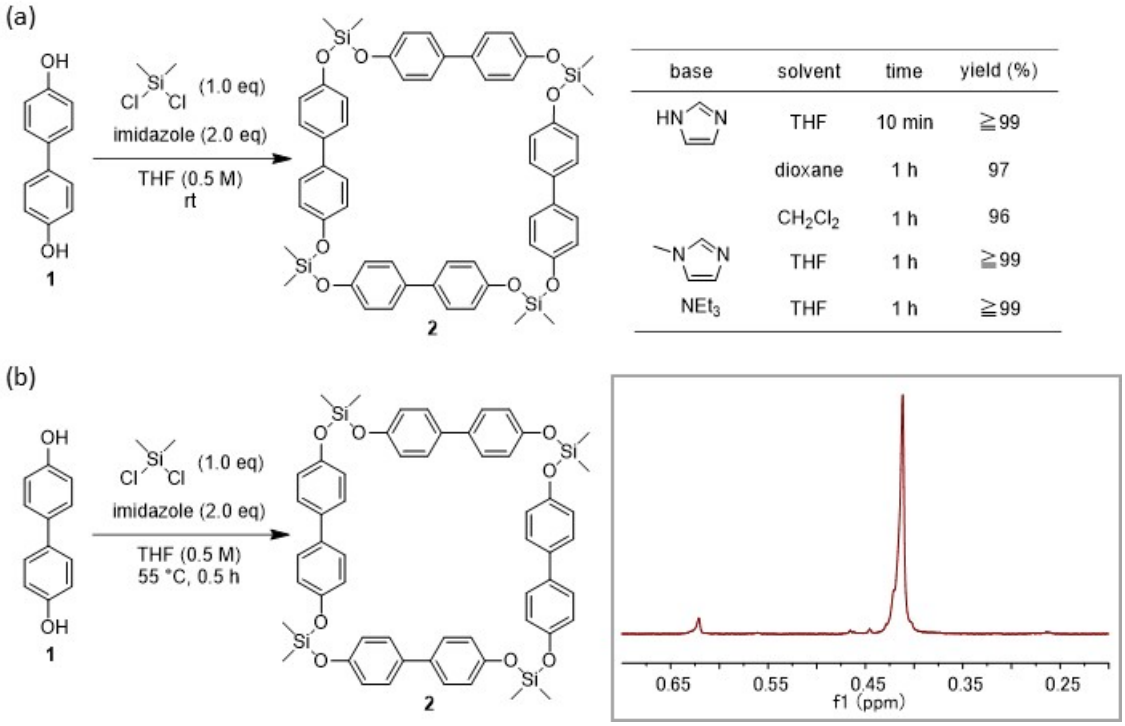

Figure S1. (a) Optimization of reaction conditions. (b) Macrocyclization was performed at 55 °C. A ^{1}H NMR spectrum indicated highly selective formation of macrocycle **2**, while formation of a small amount of a minor product likely corresponding to a different macrocyclic species was also observed.

Control Experiments with macrocycle 2

Experiment 1: To a mixture of macrocycle **2** (9.4 mg, 9.7 μmol), diol **3** (1.1 mg, 10.0 μmol) and imidazole hydrochloride (0.6 mg, 8.8 μmol) was added THF-d_8 (ca. 0.8 ml). The reaction progress was monitored by ^{1}H NMR analysis.

Experiment 2: To a suspension of macrocycle **2** (9.4 mg, 9.7 μmol) and imidazole (2.3 mg, 47.0 μmol) in THF (1.0 ml) was added dibutyldichlorosilane (5 μL, 23.2 mmol). After the mixture was stirred at room temperature for 3 h, the resulting suspension was filtered, and the solid was washed with THF. The solvent was removed under reduced pressure to afford a crude product.

Experiment 3: To a mixture of macrocycle **2** (5.6 mg, 5.8 μmol) and **4** (4.7 mg, 7.1 μmol) in THF-d_8 (ca. 0.8 ml) was added dimethyldichlorosilane (12 μL, 0.083 mmol). The reaction progress was monitored by ^{1}H NMR analysis.

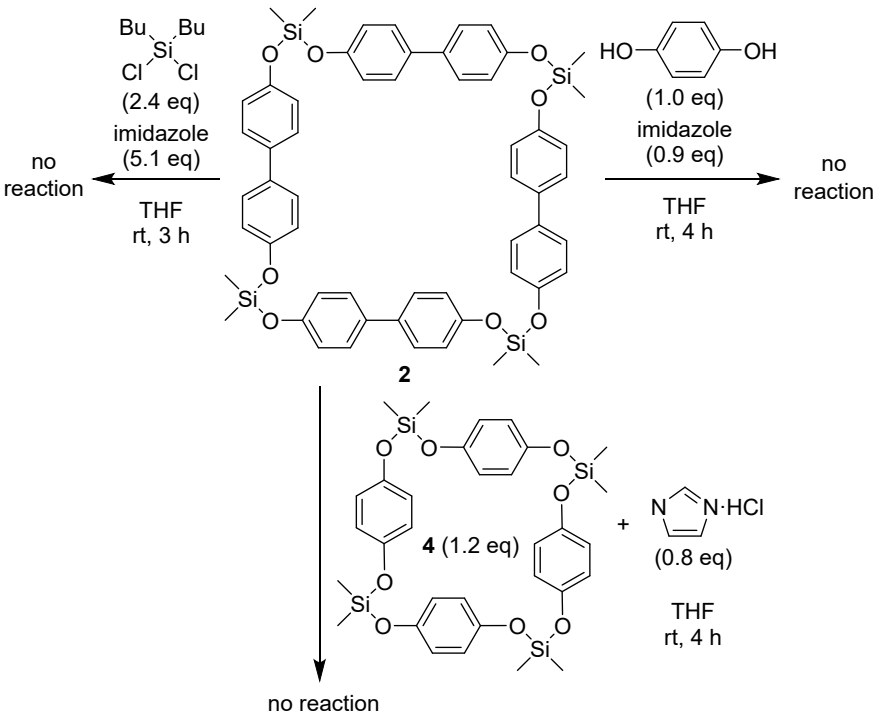

Figure S2. Studies on the dynamic behavior of the Si–O bond of macrocycle **2**.

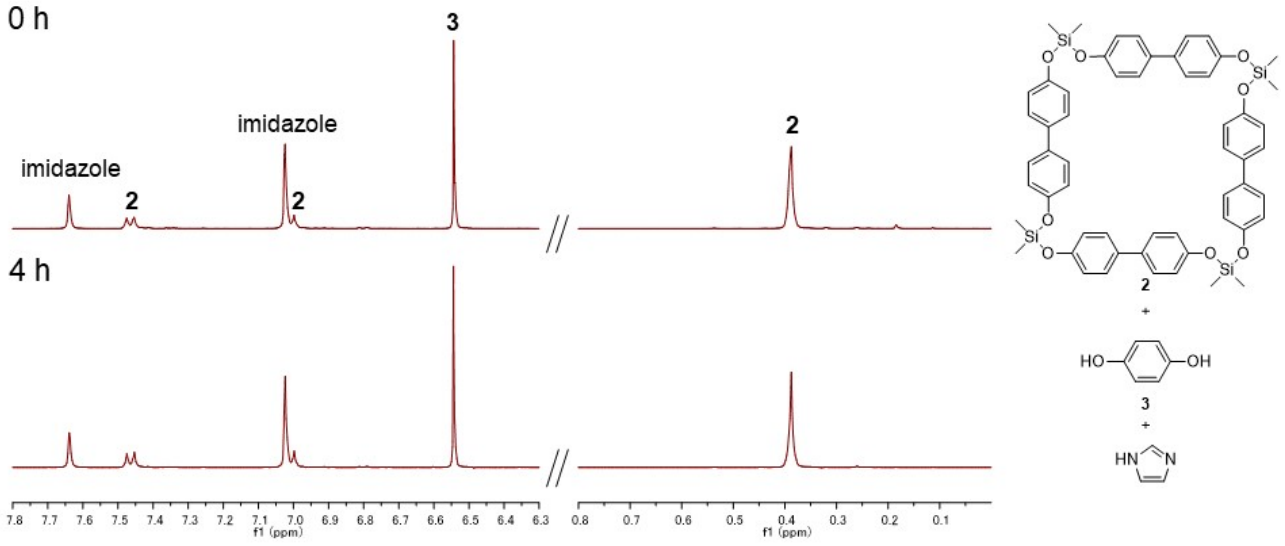

Figure S3. ^{1}H NMR spectra of a mixture of macrocycle **2**, diol **3**, and imidazole in THF-d_8. All signals did not change after 4 h, indicating that macrocycle **2** is inert toward diol under the macrocyclization conditions even in the presence of imidazole.

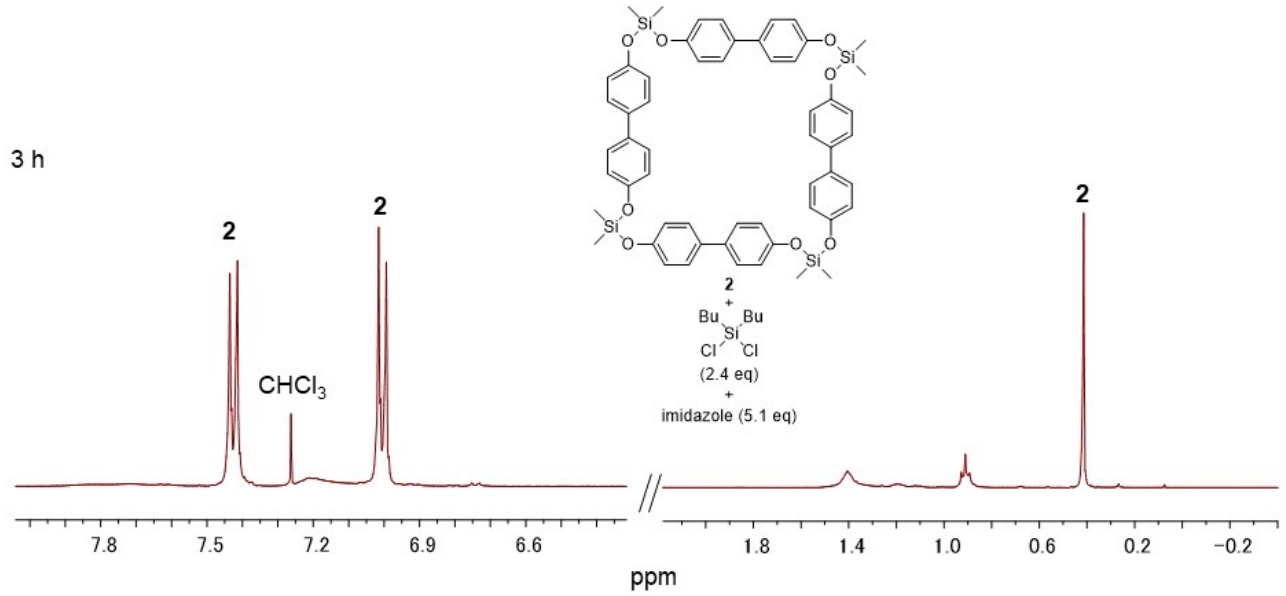

Figure S4. ^{1}H NMR spectra of a reaction of macrocycle **2** with dichlorodimethylsilane in the presence of imidazole ($CDCl_3$). All signals did not change, indicating that macrocycle **2** is inert toward diol under the macrocyclization conditions even in the presence of imidazole.

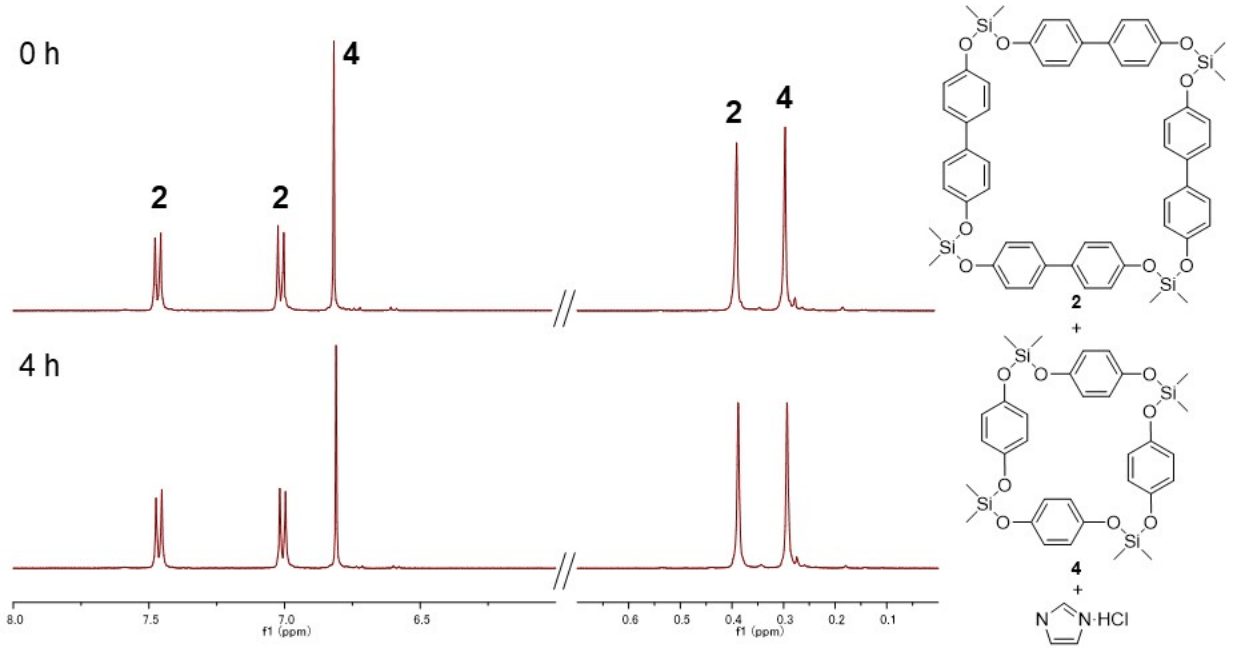

Figure S5. ^{1}H NMR spectra of a mixture of macrocycle **2** and **4** in THF-d_8.

Control Experiments with silyl ether 7

Experiment 1: To a mixture of compound **7** (6.1 mg, 0.020 mmol), diol **1** (4.7 mg, 0.025 mmol) and imidazole (2.0 mg, 0.029 mmol) was added THF-d_8 (ca. 0.8 ml). The reaction progress was monitored by ^{1}H NMR analysis.

Experiment 2: To a suspension of compound **7** (30.3 mg, 0.100 mmol) and imidazole (13.6 mg, 0.200 mmol) in

THF-d_8 (ca. 0.8 ml) was added dichlorodimethylsilane (12 μL, 0.083 mmol). After the mixture was stirred at room temperature for 1 h, the resulting suspension was filtered, and the solid was washed with THF. The solvent was removed under reduced pressure to afford a crude product.

Experiment 3: To a mixture of compound **7** (6.1 mg, 0.015 mmol), **8** (4.0 mg, 0.016 mmol) and imidazole (1.8 mg, 0.026 mmol) was added THF-d_8 (ca. 0.8 ml). The reaction progress was monitored by ^{1}H NMR analysis.

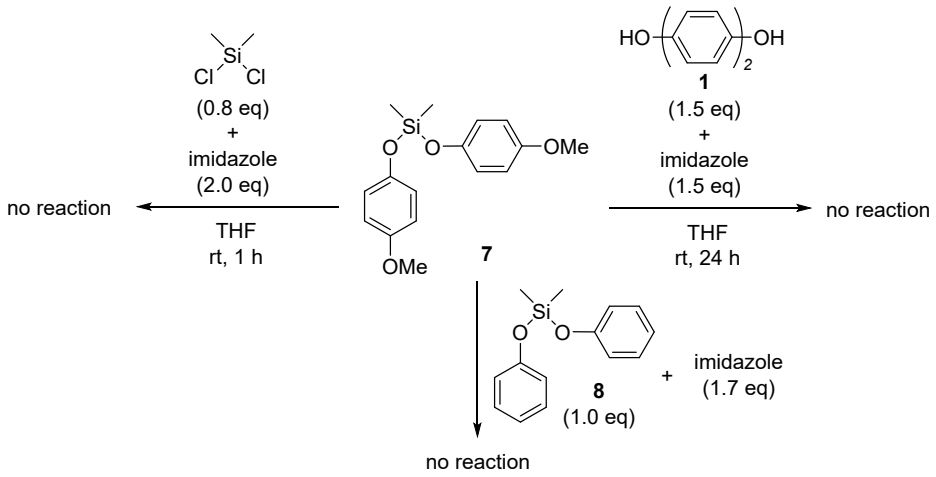

Figure S6. Studies on the dynamic behavior of the Si–O bond of silyl ether **7**.

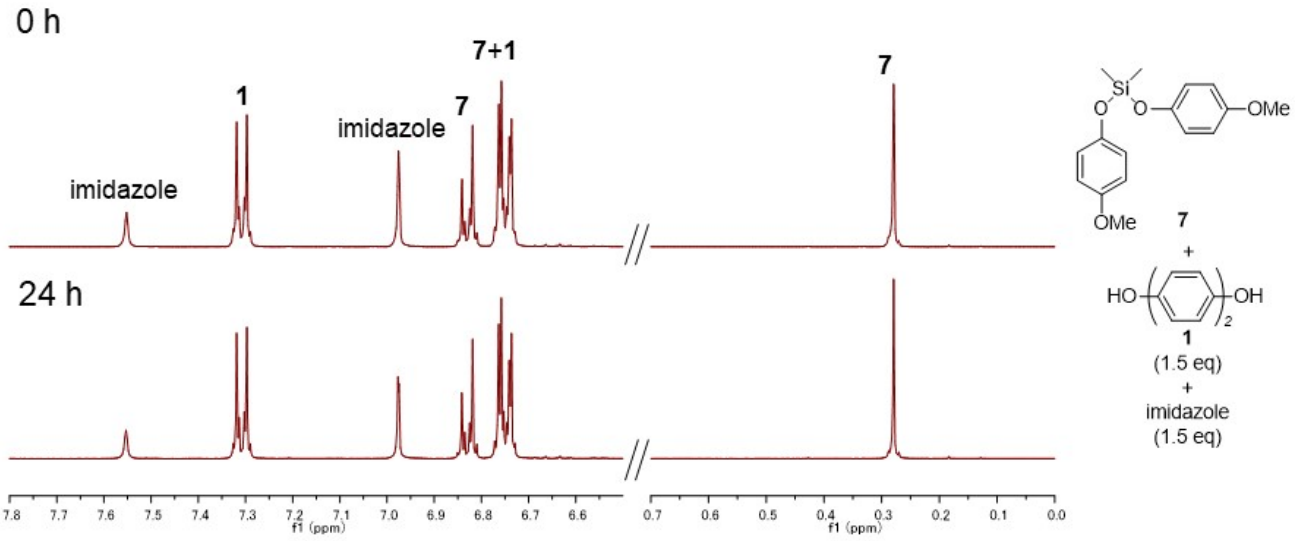

Figure S7. ^{1}H NMR spectrum of a crude product in a reaction of silyl ether **7**, diol **1**, and imidazole in THF-d_8. All signals are completely identical to the pure compounds, indicating that the silyl ether is inert toward diol even in the presence of imidazole.

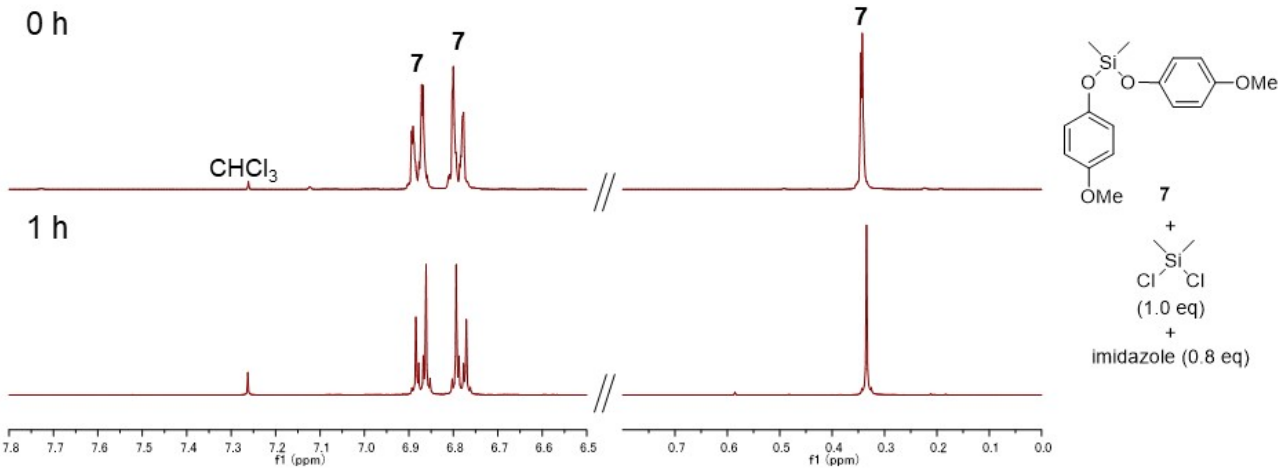

Figure S8. ^{1}H NMR spectrum of a reaction of silyl ether **7** with dichlorodimethylsilane in the presence of imidazole ($CDCl_3$). All signals did not change, indicating that the silyl ether is inert toward diol even in the presence of imidazole under the macrocyclization conditions.

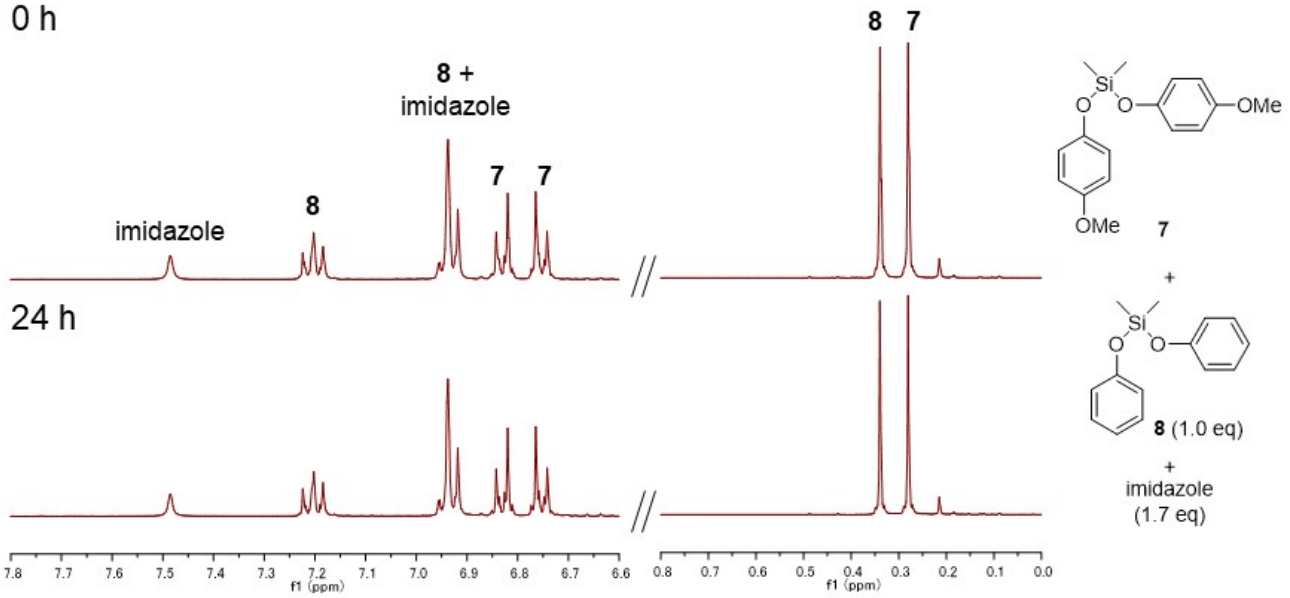

Figure S9. ^{1}H NMR spectrum of a mixture of macrocycle **7**, **8**, and imidazole in THF-d_8. All signals did not change after 24 h.

4. Single Crystal X-ray Analyses

Single crystals of **2** and **4** were obtained as described in the previous section (*vide supra*). Single-crystal X-ray diffraction data were performed at the BL02B1 beamline of SPring-8 on a PILATUS3 X CdTe 1M camera using synchrotron radiation (λ = 0.4132 Å, 30 keV) at 100(2) K temperature. All structures were integrated by using CrysAlisPro software package. The structure was determined by intrinsic phasing (SHELXT 2018/2)[S1] and refined by full-matrix least-squares refinement (SHELXL-2018/3)[S2] using the yadokari[S3] software package. Hydrogen atoms were placed in geometrically idealized positions and constrained to ride on their parent atoms. Due to severe DISORDER of the solvent molecules in **2**, the type of solvent molecule could not be determined. Therefore, the SQUEEZE routine by PLATON was used to predict the type of solvent molecules in **2**. An analysis of the structure of **2** with PLATON resulted in solvent-accessible areas of 708 Å^3. The SQUEEZE program was used to calculate and correct for electron density (140 e$^-$/cell) identified in a solvent-accessible area. As Et_2O was used as the solvent, and if possesses 42 e$^-$, equating to 4 diethyl ether molecules per asymmetric unit. We tried to refine the disordered Et_2O in compound **2** again. Similarity restraints (SIMU) have been applied to the anisotropic displacement parameters of the Et_2O molecule. The anisotropic displacement parameters of Et_2O carbon and oxygen atoms have been restrained to have more isotropic character (ISOR). The refinement crystallographic details of **2** and **4** are summarized in Table S1.

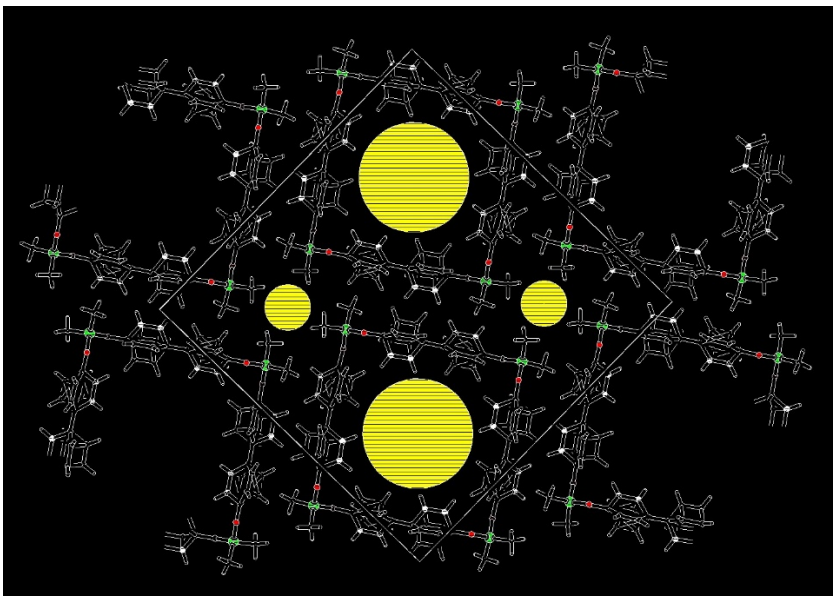

Figure S10. The total free volume of the macrocycle **2** after the removal of guest molecules are 22.2% (i.e., 703.5 Å^3 of the unit cell volume of 3175.1 Å^3) as estimated using PLATON.

Table S1. X-ray Crystallographic Data for **2** and **4**.

	2 before SQUEEZE	**2 after SQUEEZE**	**4**
CCDC		2347140	2347141
formula	$C_{56}H_{56}O_8Si_4$,4Et_2O	$C_{56}H_{56}O_8Si_4$	$C_{32}H_{40}O_8Si_4$

fw	1265.84	969.36	665.00
crystal dimension (mm)	0.01 × 0.01 × 0.01	0.01 × 0.01 × 0.01	0.02 × 0.02 × 0.01
Temp. (K)	100(2)	100(2)	100(2)
crystal system	tetragonal	tetragonal	monoclinic
space group	*P*4/*n*	*P*4/*n*	$P2_1/c$
a, Å	24.8118(5)	24.8118(5)	13.3626(5)
b, Å	24.8118(5)	24.8118(5)	10.5370(2)
c, Å	5.1576(2)	5.1576(2)	12.8771(4)
α, deg	90	90	90
β, deg	90	90	112.376(4)
γ, deg	90	90	90
V, Å^3	3175.15(18)	3175.15(18)	1676.60(10)
Z	2	2	2
ρ_{calcd}, g cm^{-3}	1.324	1.014	1.317
F(000)	1360	1024	704
μ, cm^{-1}	0.52	0.42	0.64
transmission factors (min.)	0.89985	0.89985	0.45408
index range	-31 ≤ h ≤ 31	-30 ≤ h ≤ 30	-16 ≤ h ≤ 16
	-31 ≤ k ≤ 31	-30 ≤ k ≤ 30	-13 ≤ k ≤ 13
	-6 ≤ l ≤ 6	-6 ≤ l ≤ 6	-16 ≤ l ≤ 16
no. reflections total	60564	60564	23065
unique (R_{int})	3253 (0.1281)	3253 (0.1178)	3406 (0.0944)
$I > 2\sigma(I)$	2443	2777	2718
no. parameters	274	229	203
R1 ($I > 2\sigma(I)$)[a]	0.0678	0.0524	0.0456
wR2 (all data)[b]	0.2235	0.1205	0.1206
GOF [c]	1.056	1.194	1.028
max diff peak / hole, e Å^{-3}	0.837/-0.427	0.231/-0.232	0.75/-0.34

[a] $R1 = \Sigma||F_o| - |F_c||/\Sigma|F_o|$. [b] $wR2 = [\Sigma\{w(F_o^2 - F_c^2)^2\}/\Sigma w(F_o^2)^2]^{1/2}$, $w = 1/[\sigma^2 F_o^2 + (aP)^2 + bP]$ (a and b are constants suggested by the refinement program; $P = [\max(F_o^2,0) + 2F_c^2]/3$). [c] $GOF = [\Sigma w(F_o^2 - F_c^2)^2/(N_{obs} - N_{params})]^{1/2}$.

5. DFT Calculations

All calculations were carried out by using the Gaussian 16 program packages.[S5] Geometry optimizations were performed at B3LYP/6-311Gd with GD3BJ empirical dispersion.[S6] A potential energy surface of the model compound was calculated by scanning the torsion angles of C_{Ph}–O–Si–O′ (θ) and C_{Ph}′–O′–Si–O (θ′). Non-covalent interactions were evaluated by using the NCIPLOT program package.[S7]

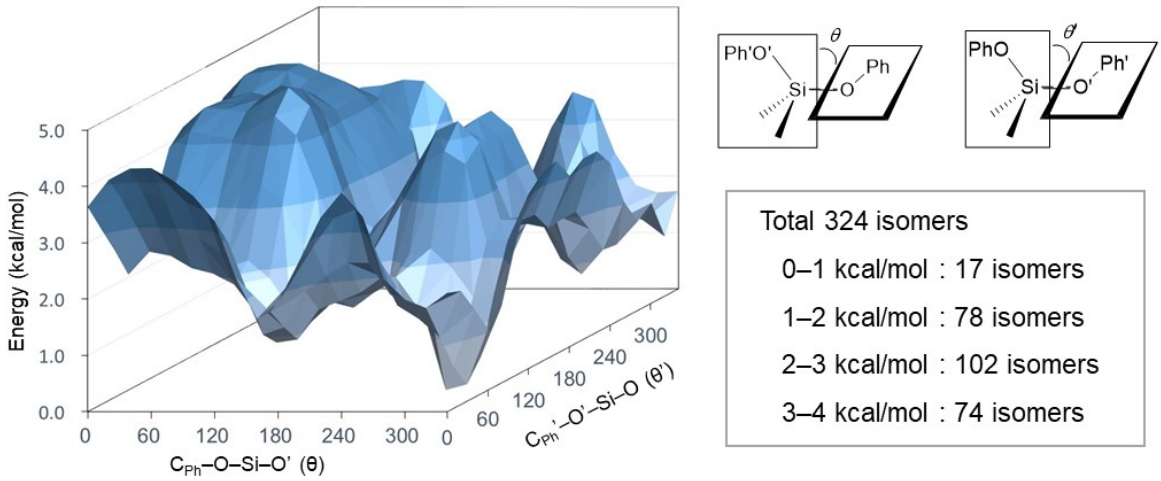

Figure S11. An energy landscape of $Me_2Si(OPh)_2$ calculated as a function of the torsion angles of C_{Ph}–O–Si–O′ (θ) and C_{Ph}′–O′–Si–O (θ′).

6. References

S1. Sheldrick, G. M. *Acta Crystallogr. Sect. A,* **2015**, *71*, 3-8.

S2. Sheldrick, G. M. *Acta Crystallogr. Sect. C,* **2015**, *71*, 3-8.

S3. Yadokari-XG, Software for Crystal Structure Analyses, K. Wakita (2001); Release of Software (Yadokari-XG 2009) for Crystal Structure Analyses, C. Kabuto, S. Akine, T. Nemoto, and E. Kwon, *J. Cryst. Soc. Jpn.,* **2009**, *51*, 218-224 (2009).

S4. Spek, A. L. *Acta Cryst. Sect. D,* **2009**, *65*, 145-155.

S5. Frisch, M. J.; Trucks, G. W.; Schlegel, H. B.; Scuseria, G. E.; Robb, M. A.; Cheeseman, J. R.; Scalmani, G.; Barone, V.; Petersson, G. A.; Nakatsuji, H.; Li, X.; Caricato, M.; Marenich, A. V.; Bloino, J.; Janesko, B. G.; Gomperts, R.; Mennucci, B.; Hratchian, H. P.; Ortiz, J. V.; Izmaylov, A. F.; Sonnenberg, J. L.; Williams; Ding, F.; Lipparini, F.; Egidi, F.; Goings, J.; Peng, B.; Petrone, A.; Henderson, T.; Ranasinghe, D.; Zakrzewski, V. G.; Gao, J.; Rega, N.; Zheng, G.; Liang, W.; Hada, M.; Ehara, M.; Toyota, K.; Fukuda, R.; Hasegawa, J.; Ishida, M.; Nakajima, T.; Honda, Y.; Kitao, O.; Nakai, H.; Vreven, T.; Throssell, K.; Montgomery Jr., J. A.; Peralta, J. E.; Ogliaro, F.; Bearpark, M. J.; Heyd, J. J.; Brothers, E. N.; Kudin, K. N.; Staroverov, V. N.; Keith, T. A.; Kobayashi, R.; Normand, J.; Raghavachari, K.; Rendell, A. P.; Burant, J. C.; Iyengar, S. S.; Tomasi, J.; Cossi, M.; Millam, J. M.; Klene, M.; Adamo, C.; Cammi, R.; Ochterski, J. W.; Martin, R. L.; Morokuma, K.; Farkas, O.; Foresman, J. B.; Fox, D. J. Gaussian 16 Rev. C.01, Wallingford, CT, 2016.

S6. (a) Grimme, S. *J. Comp. Chem.*, **2006**, *27*, 1787−1799. (b) Grimme, S.; Ehrlich, S.; Goerigk, L. *J. Comp. Chem*. **2011**, *32*, 1456−1465.

S7. Contreras-García, J.; Johnson, E. R.; Keinan, S.; Chaudret, R.; Piquemal, J. P.; Beratan, D. N.;Yang, W., NCIPLOT: A Program for Plotting Noncovalent Interaction Regions. *J. Chem. Theory Comput.* 2011, *7*, 625−632.

7. NMR Spectra

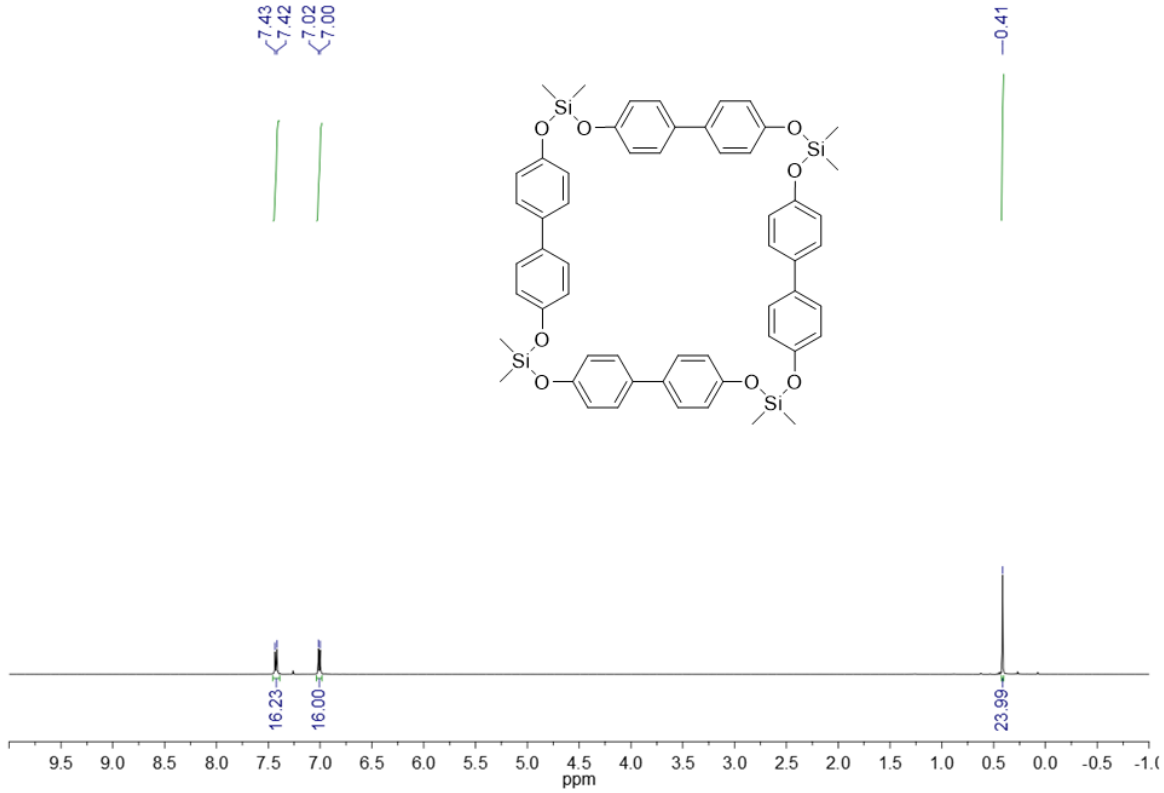

Figure S12. ^{1}H NMR spectrum of **2** in $CDCl_3$ (500 MHz).

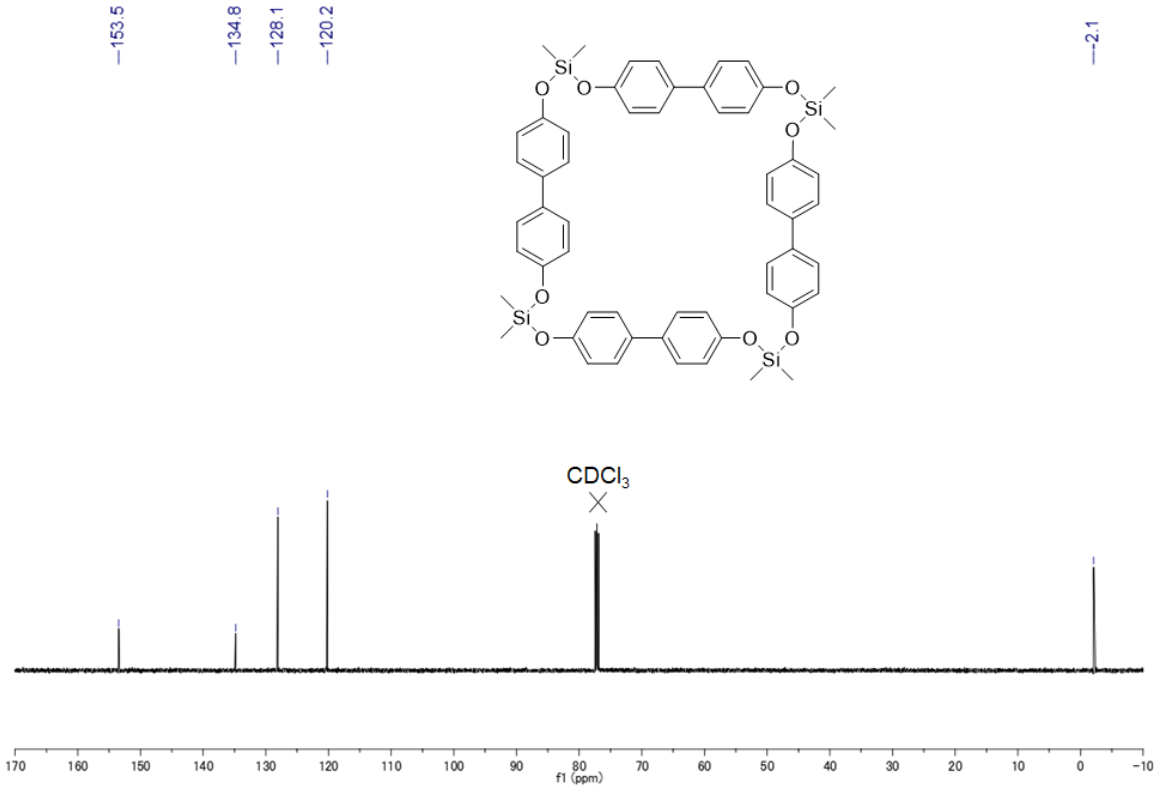

Figure S13. $^{13}C\{^{1}H\}$ NMR spectrum of **2** in $CDCl_3$ (100 MHz).

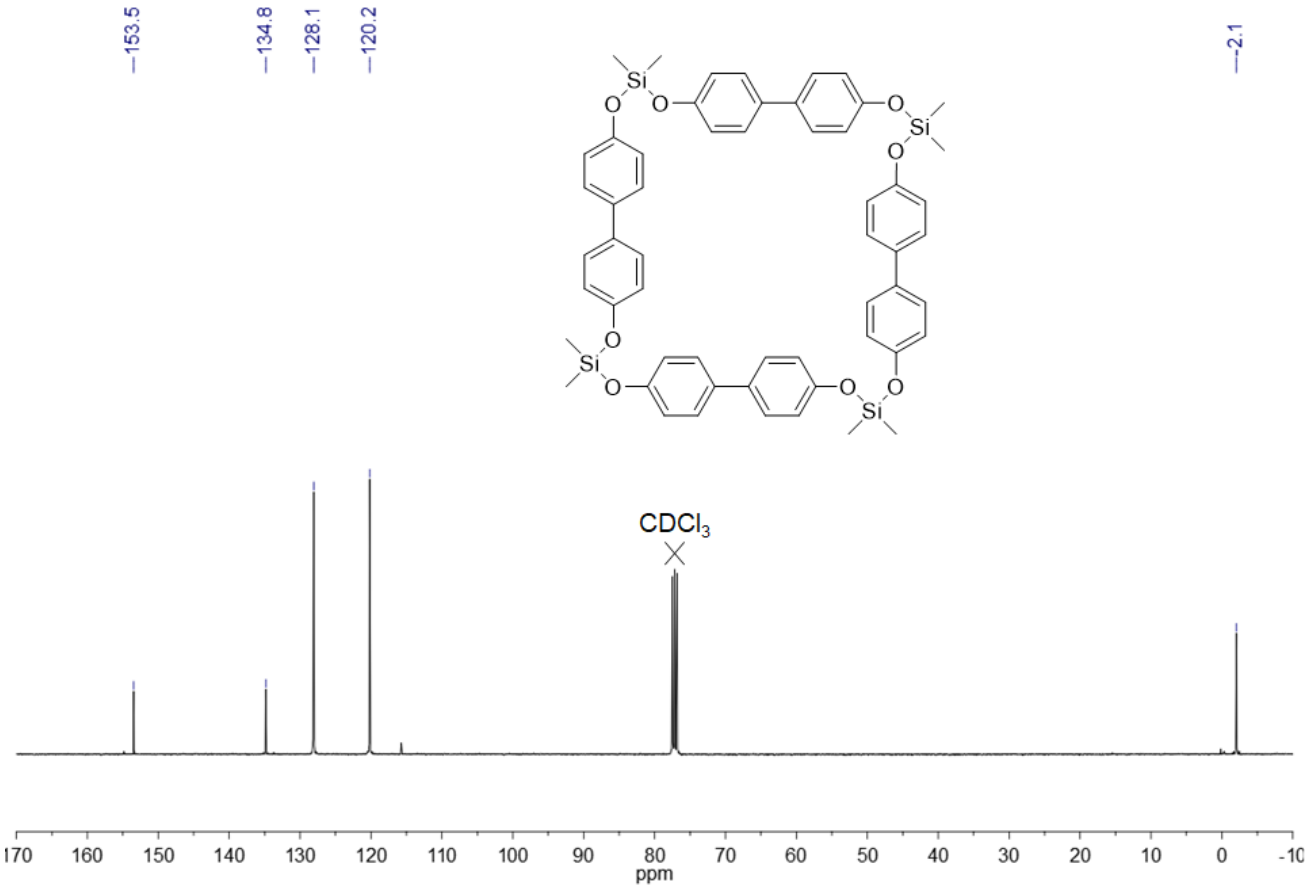

Figure S14. $^{13}C\{^{1}H\}$ NMR of the product obtained by a reaction at a concentration of 3.0 M in $CDCl_3$ (125 MHz).

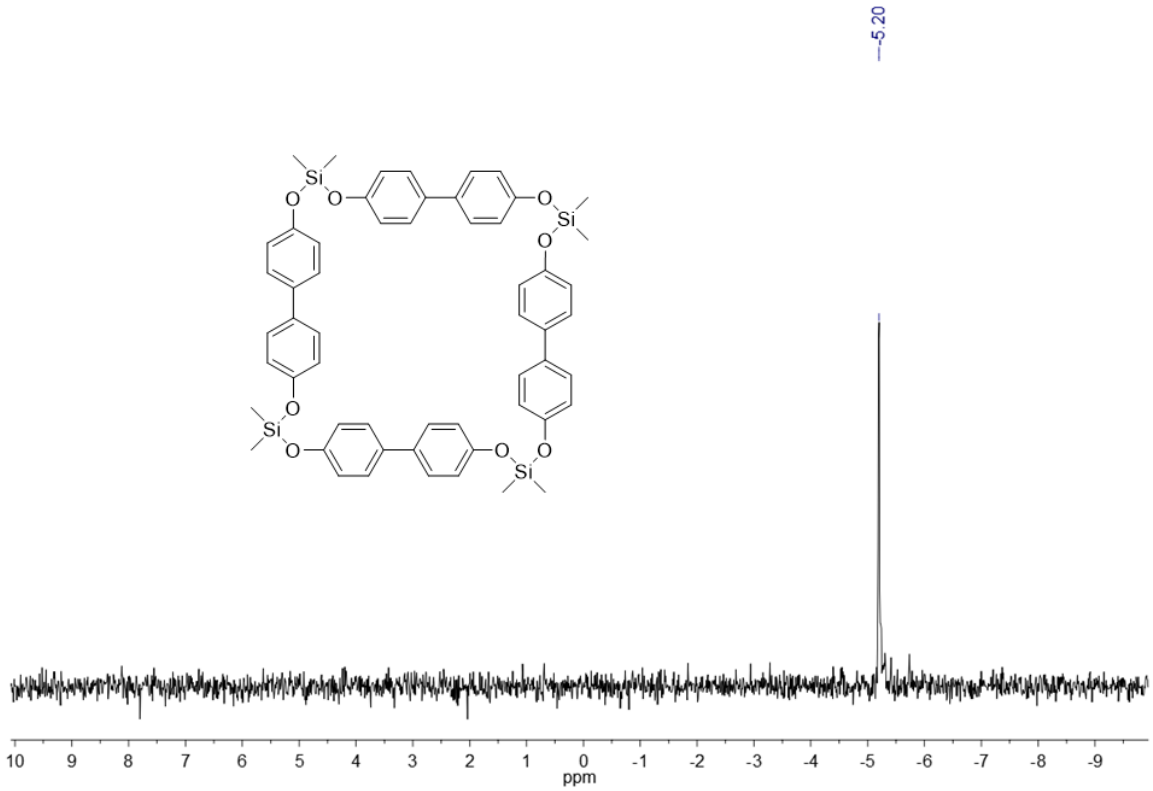

Figure S15. $^{29}Si\{^{1}H\}$ NMR spectrum of **2** in $CDCl_3$ (79 MHz).

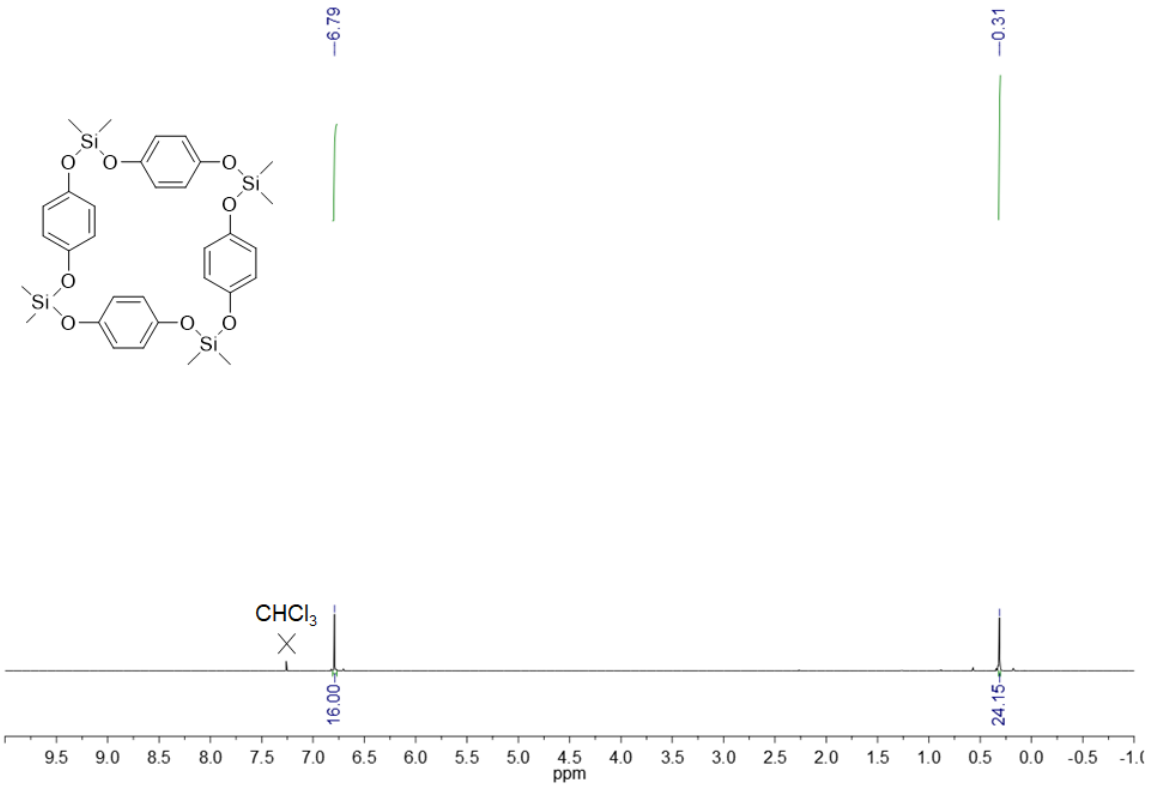

Figure S16. ^{1}H NMR spectrum of **4** in $CDCl_3$ (400 MHz).

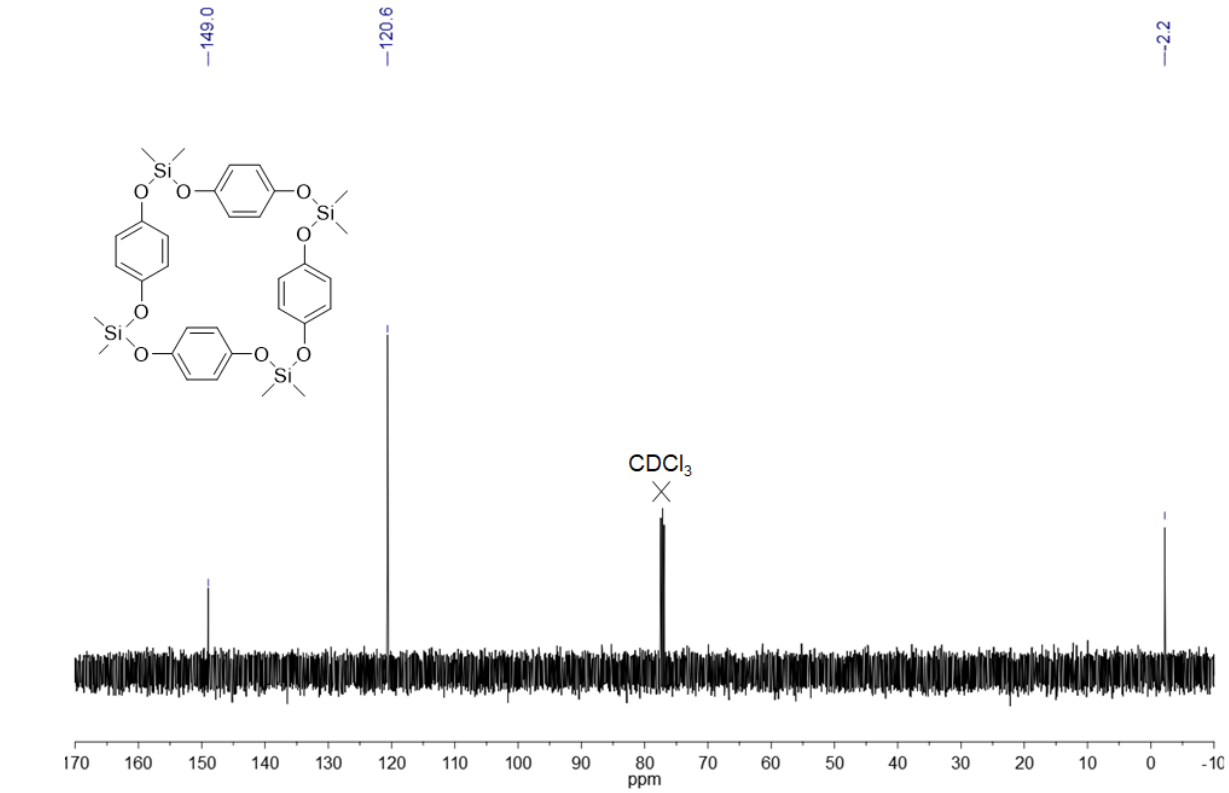

Figure S17. $^{13}C\{^{1}H\}$ NMR spectrum of **4** in $CDCl_3$ (125 MHz).

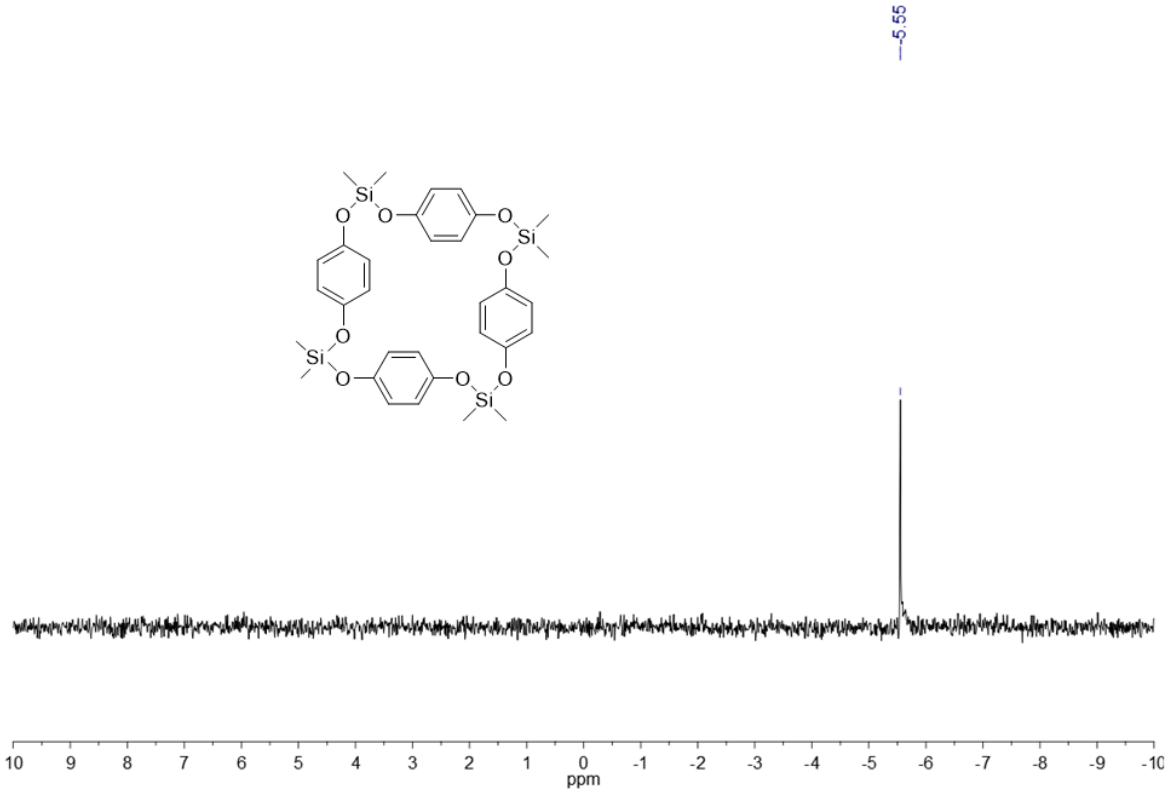

Figure S18. $^{29}Si\{^{1}H\}$ NMR spectrum of **4** in $CDCl_3$ (79 MHz).

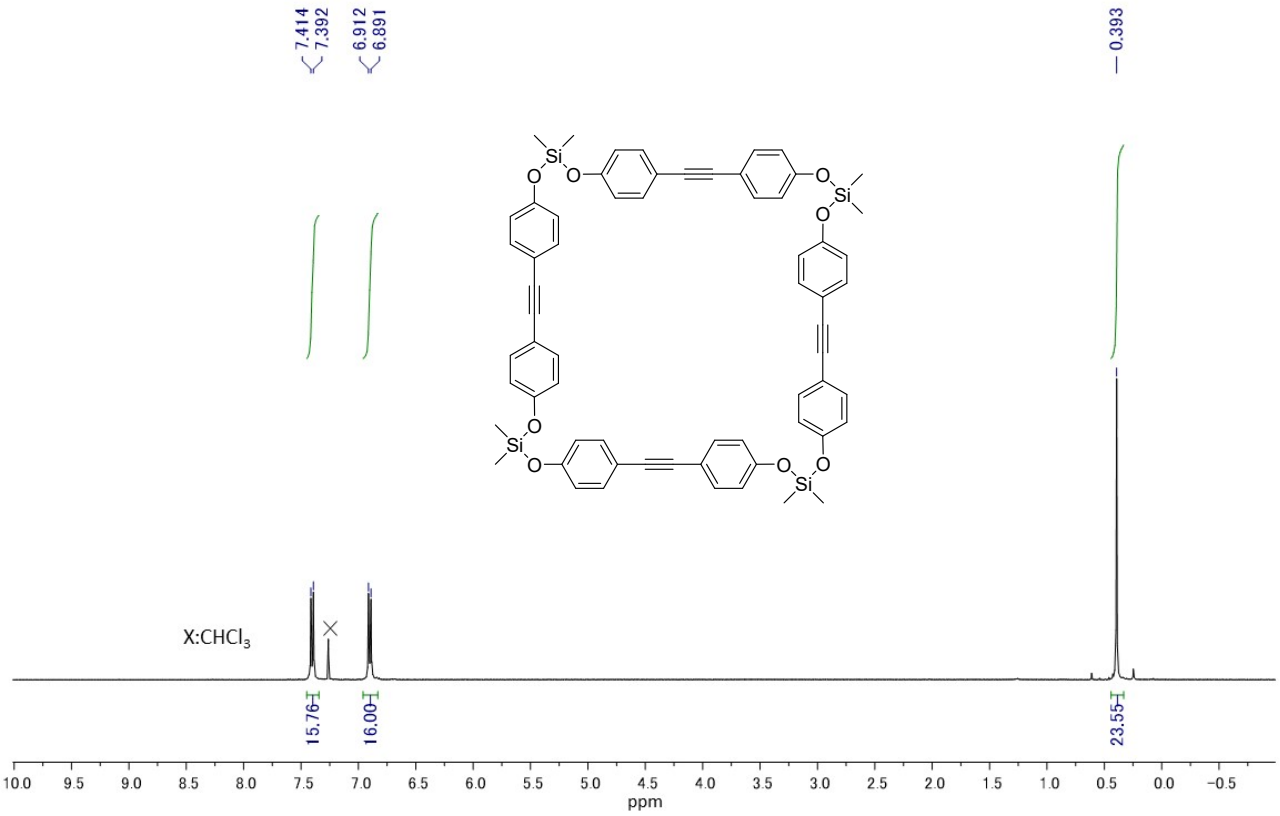

Figure S19. ^{1}H NMR spectrum of **6** in $CDCl_3$ (400 MHz).

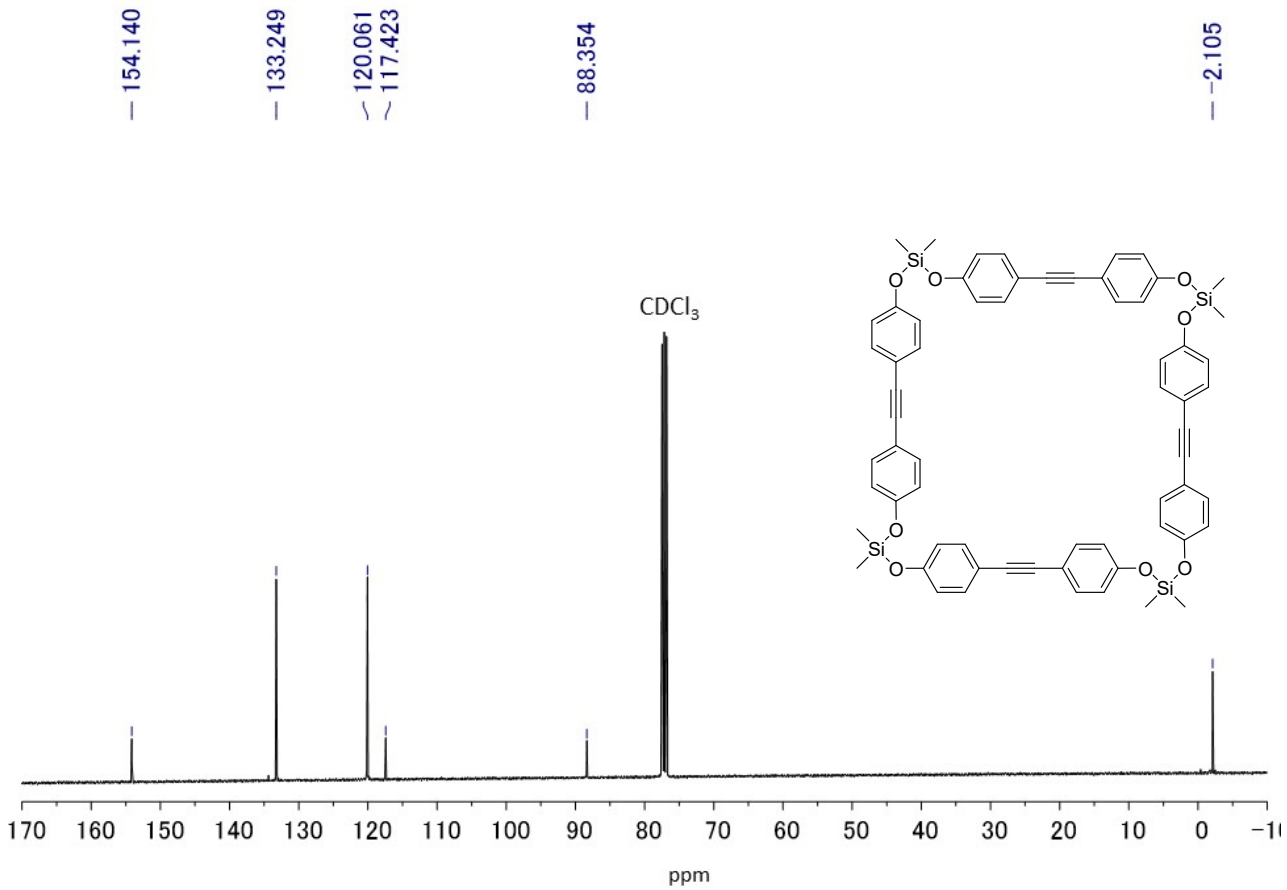

Figure S20. $^{13}C\{^{1}H\}$ NMR spectrum of **6** in $CDCl_3$ (100 MHz).

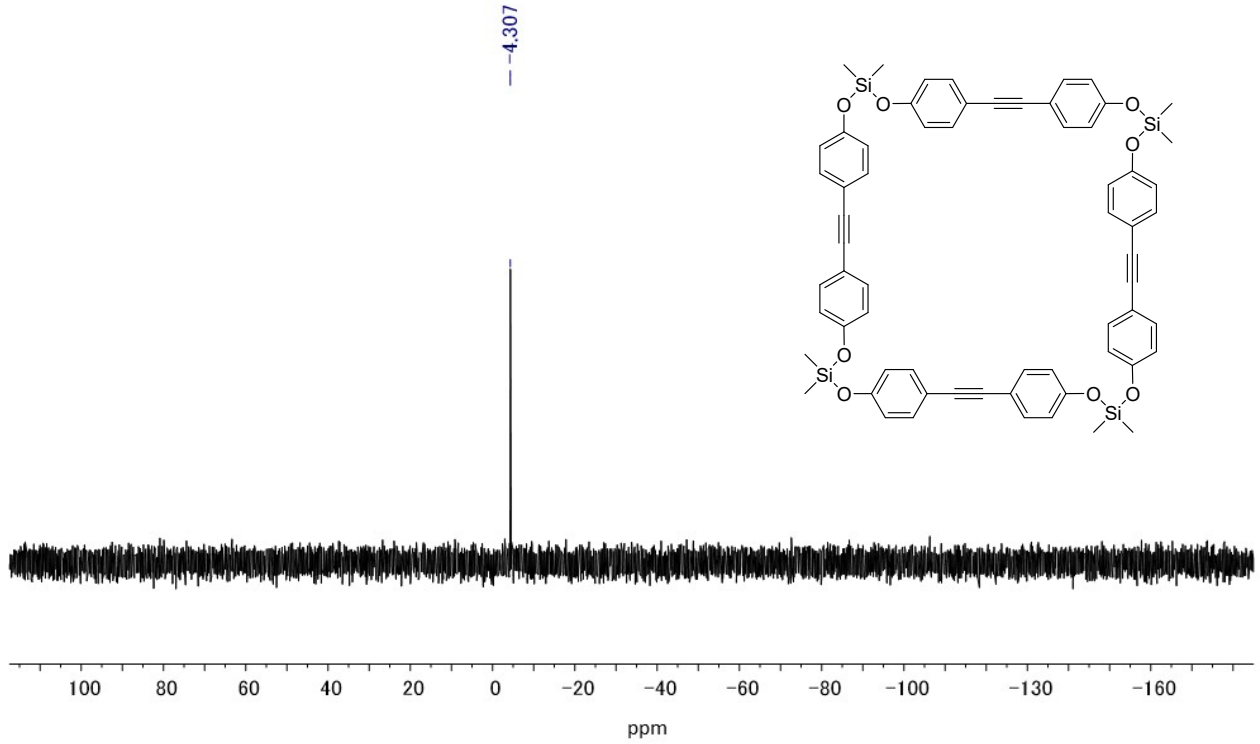

Figure S21. ^{29}Si DEPT NMR spectrum of **6** in $CDCl_3$ (79 MHz).

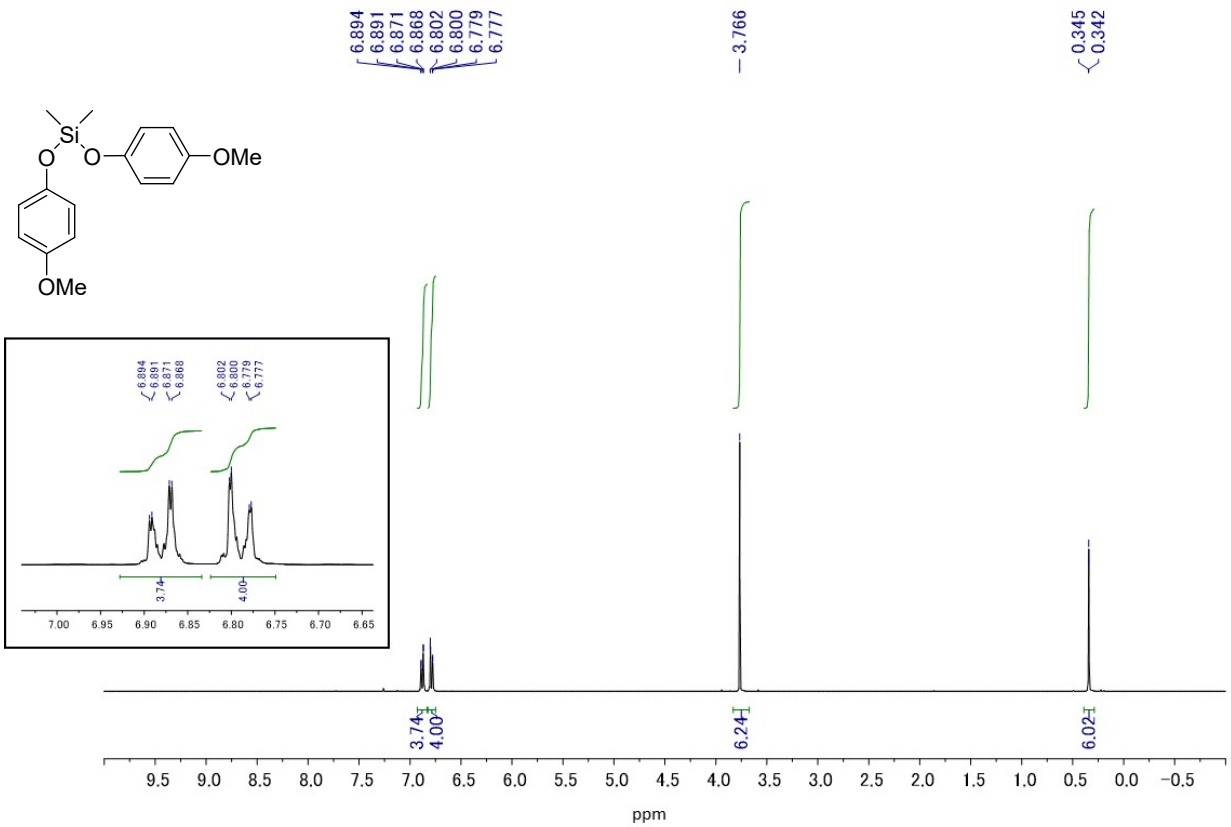

Figure S22. ^{1}H NMR spectrum of **7** in $CDCl_3$ (400 MHz).

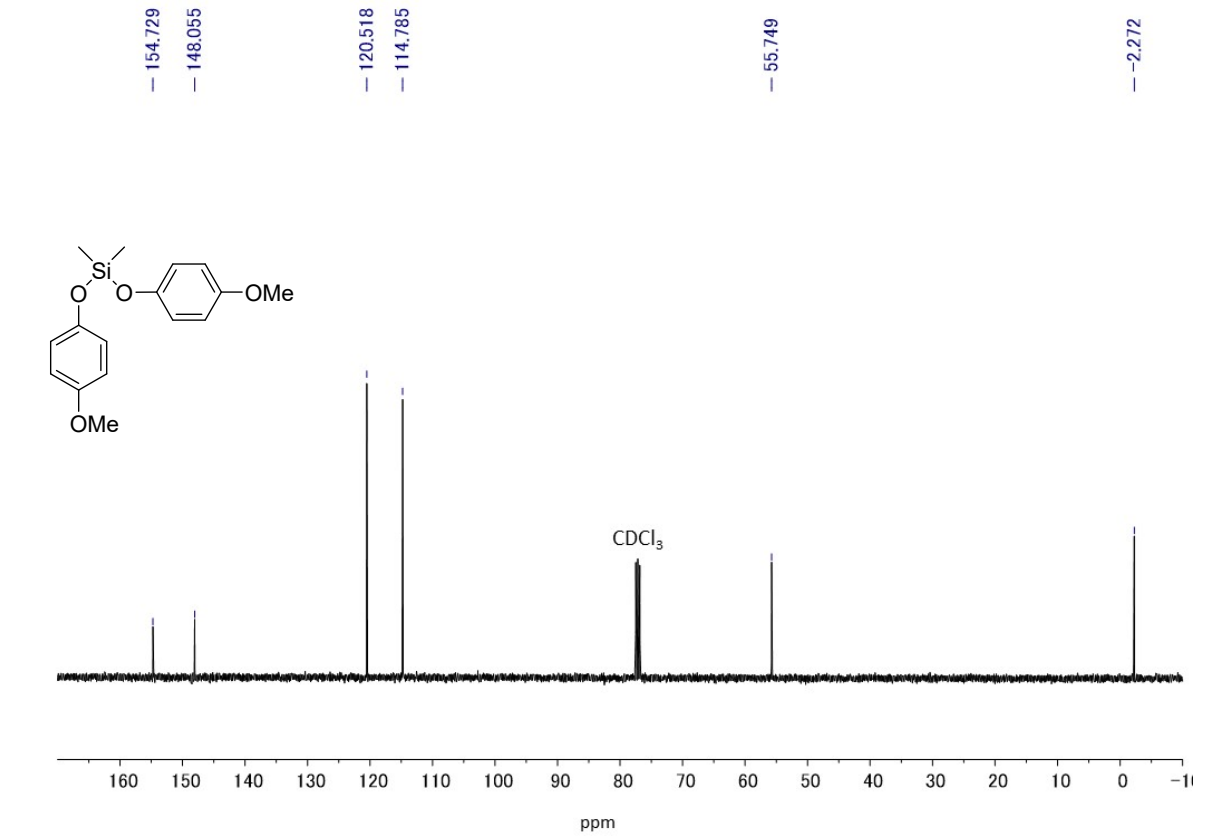

Figure S23. ^{13}C NMR spectrum of **7** in $CDCl_3$ (100 MHz).

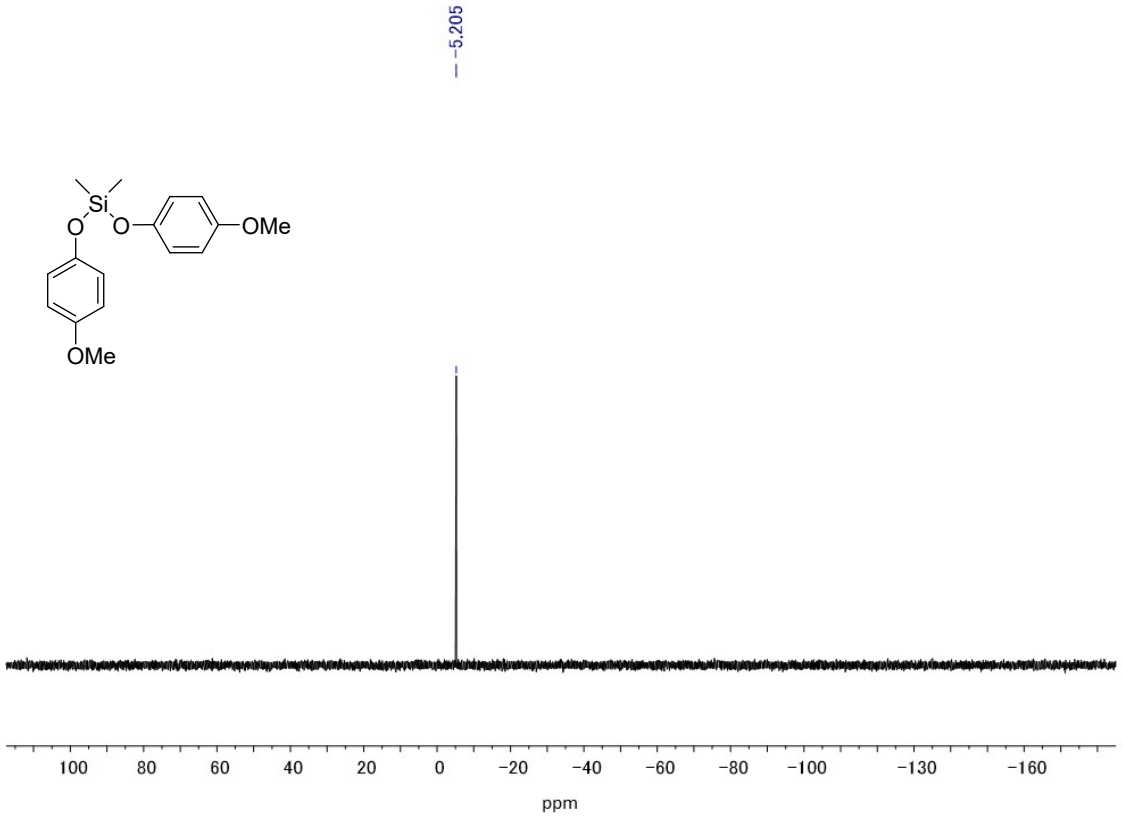

Figure S24. ^{29}Si DEPT NMR spectrum of **7** in $CDCl_3$ (79 MHz).

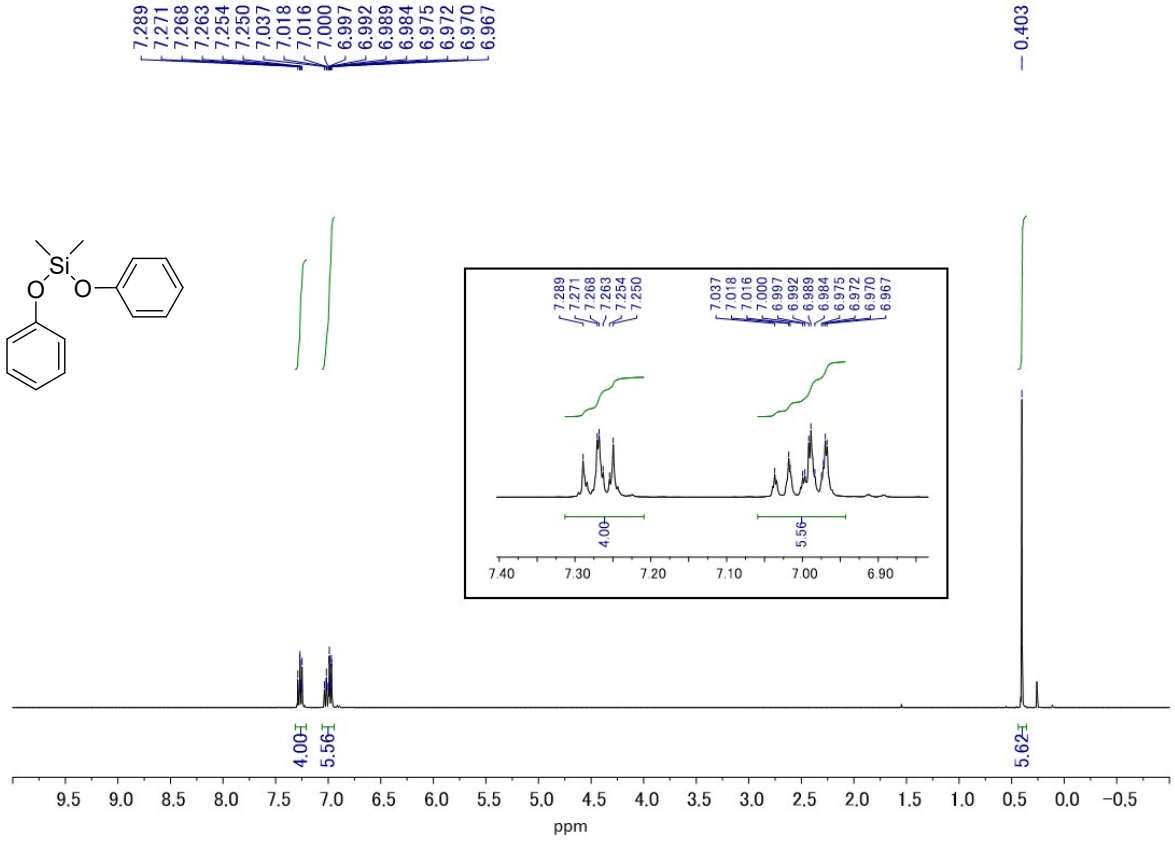

Figure S25. ^{1}H NMR spectrum of **8** in $CDCl_3$ (400 MHz).

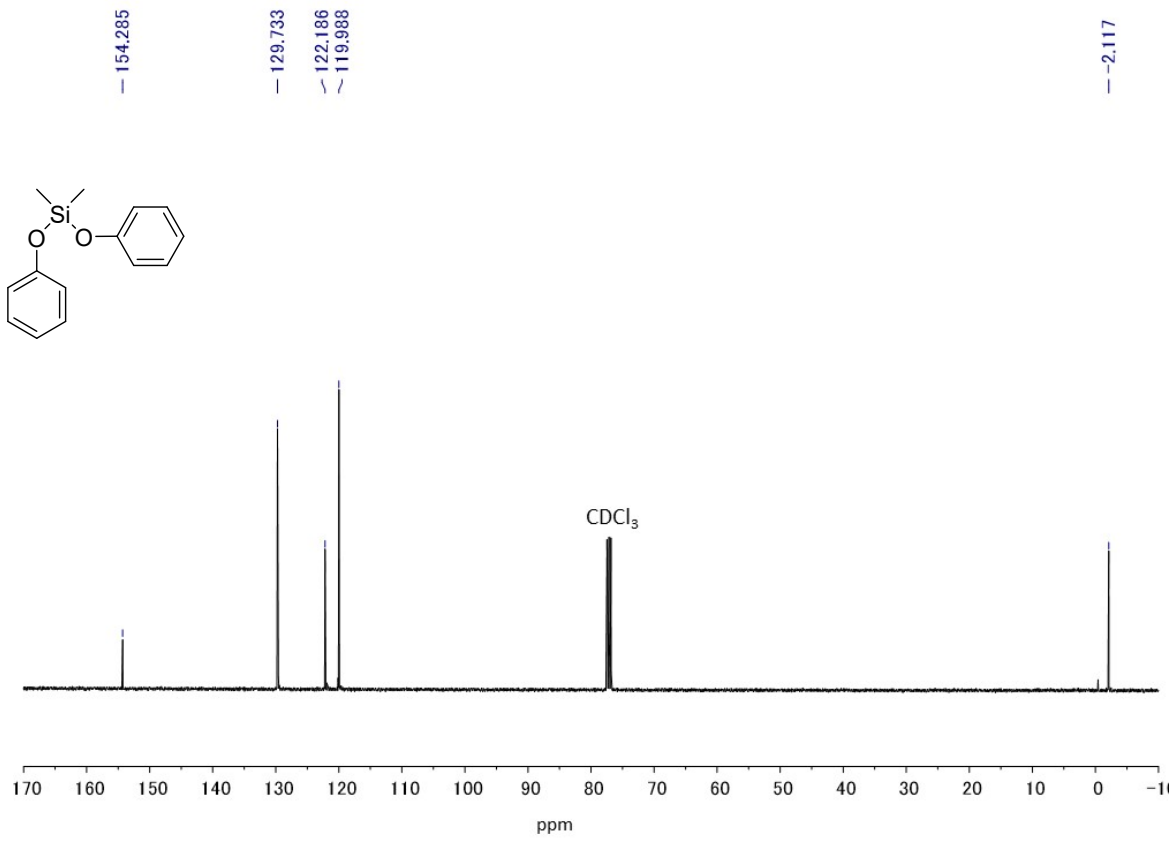

Figure S26. $^{13}C\{^{1}H\}$ NMR spectrum of **8** in $CDCl_3$ (100 MHz).

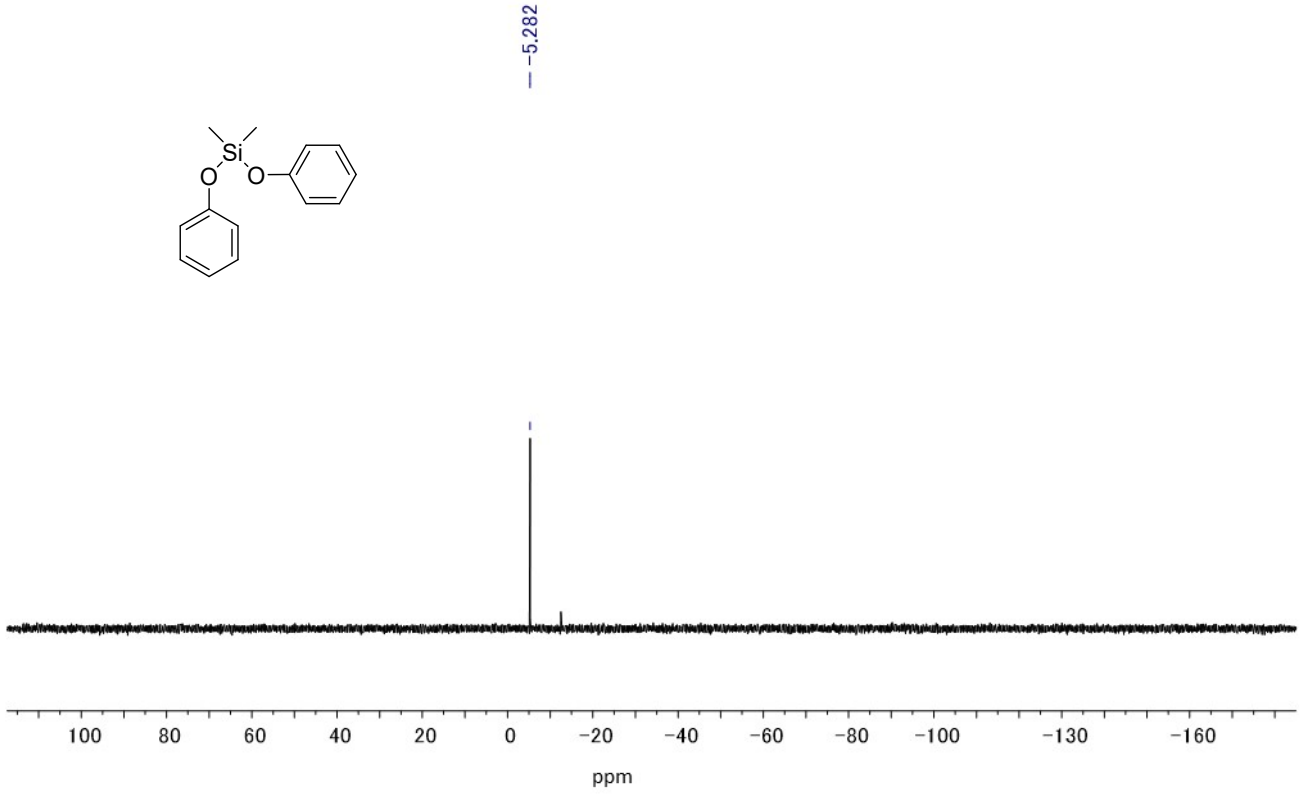

Figure S27. ^{29}Si DEPT NMR spectrum of **8** in $CDCl_3$ (79 MHz).